Chinese Journal of Aeronautics, (2014),27(5): 1180–1187

Chinese Society of Aeronautics and Astronautics
& Beihang University

Chinese Journal of Aeronautics

cja@buaa.edu.cn
www.sciencedirect.com

Determination of thermal expansion coefficients for unidirectional fiber-reinforced composites

Ran Zhiguo, Yan Ying *, Li Jianfeng, Qi Zhongxing, Yang Lei

School of Aeronautics Science and Engineering, Beihang University, Beijing 100191, China

Received 3 September 2013; revised 13 November 2013; accepted 10 February 2014
Available online 19 March 2014

KEYWORDS

Analytical solution;
Coefficient of thermal expansion;
Thermo-elastic;
Transversely isotropic;
Unidirectional composites

Abstract In the present work, the coefficients of thermal expansion (CTEs) of unidirectional (UD) fiber-reinforced composites are studied. First, an attempt is made to propose a model to predict both longitudinal and transverse CTEs of UD composites by means of thermo-elastic mechanics analysis. The proposed model is supposed to be a concentric cylinder with a transversely isotropic fiber embedded in an isotropic matrix, and it is subjected to a uniform temperature change. Then a concise and explicit formula is offered for each CTE. Finally, some finite element (FE) models are created by a finite element program MSC. Patran according to different material systems and fiber volume fractions. In addition, the available experimental data and results of other analytical solutions of CTEs are presented. Comparisons are made among the results of the cylinder model, the finite element method (FEM), experiments, and other solutions, which show that the predicted CTEs by the new model are in good agreement with the experimental data. In particular, transverse CTEs generally offer better agreements than those predicted by most of other solutions.

1. Introduction

As we know, composite materials have been undergoing extraordinary technological advances and enjoying widespread applications in different fields. However, as a result of their complex properties, such as wettability, chemical compatibility, anisotropic mechanics, heat absorption and conductivity abilities, their complete characterization has not been achieved so far.

Coefficient of thermal expansion (CTE) is defined as the fractional change in length of a body under heating or cooling through a given temperature range,[1] and it is usually given as a coefficient per unit temperature interval at a given temperature. It is a key material property especially when a composite structure works in a temperature-changing environment. Here, the focus was placed upon on studying the longitudinal and transverse CTEs of continuous fiber-reinforced unidirectional (UD) composites.

The problem of relating effective properties of a fiber-reinforced material to its constituent properties has drawn great attention. As a result, many analytical solutions have been made to predict the upper and lower bounds of CTEs of UD composites, which are composed of isotropic or anisotropic

* Corresponding author. Tel.: +86 10 82315947.
E-mail addresses: mfdickl1@163.com (Z. Ran), yingyan@buaa.edu.cn (Y. Yan).

Peer review under responsibility of Editorial Committee of CJA.

http://dx.doi.org/10.1016/j.cja.2014.03.010

fibers and matrices.[2–12] In a series of studies by van Fo Fy,[3–5] analytical solutions were presented to predict both axial and transverse CTEs of a UD composite through its constituent properties. However, the results were very sensitive to the elastic modulus and Poisson's ratio of the UD material. Levin[6] expanded Hill's method and gave the upper bounds of a certain glass fiber-reinforced composite's CTEs, and the results were in much better agreement with the data in Van Fo Fy's study[3] than other predictions in that paper. Schapery[2] has derived expressions for longitudinal and transverse CTEs of composites with isotropic fibers embedded in isotropic matrices by adopting extreme energy principles. Sideridis[12] and Chamis[9] applied different methods and obtained the same longitudinal CTE expression, while the transverse expressions were quite different. In general, the predictions of longitudinal CTEs were always in good agreement with experimental data, while those of transverse CTEs failed to agree. An exception was Rosen and Hashin's prediction[10] as an extension of the work of Levin.[6] However, it is inconvenient to obtain results by Rosen and Hashin's solution, because to solve the CTEs of a composite, the mechanical properties of both the composite and its constituents must be determined first.

At the same time, as computation capability has grown dramatically over the last three decades, numerical solutions such as the finite element method (FEM) are being extensively applied to determine the CTEs of composite materials. Islam[13] and Rupnowski et al.[14] investigated the linear CTEs of UD composites systematically by the FEM. Karadeniz et al.[15] explored the CTEs of different material systems by micromechanical modeling using the FEM, and comparisons were carried out among their results, analytical solutions, and experimental data. However, discrepancies still exist between FEM results and experimental data.

Generally, the transverse CTE prediction of a UD composite was not as good as that of the longitudinal CTE. However, an exact transverse CTE of a UD composite is rather important in designing high-dimensional stable structures. Therefore, we tried to achieve a practical solution of CTEs by doing thermo-elastic analysis in this paper, especially the transverse CTE was paid much attention to. In addition, results of analytical solutions, the FEM, and experiments available in literatures were compared for justifications.

2. Theoretical analysis

2.1. Proposed model

The cross-section of a UD fiber-reinforced composite is shown in Fig. 1, and a typical representative volume element (RVE) could be a cylinder fiber embedded in a cube, in which the cylinder stands for the fiber, while the cube symbolizes the matrix.

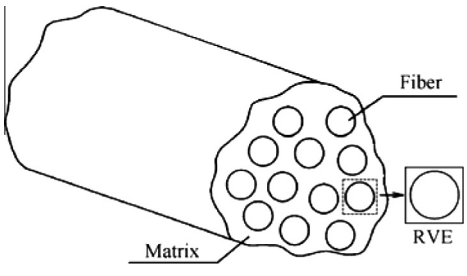

Fig. 1 Cross-section of UD fiber-reinforced composite.

To make this thermo-elastic analysis easier, the cubic RVE is transformed into a concentric cylinder model (see Fig. 2) according to the following assumptions: (1) both the cubic model and the cylinder model have the same fiber radius; (2) two models with the same fiber volume fraction; (3) two models with the same length in the longitudinal direction.

Consider that the radius of the fiber r_1, the fiber volume fraction V_f, and the length of the RVE h are all known.

The cross-section of the cubic model is defined by a circle with a radius of r_1 surrounded by a $2l \times 2l$ square (see Fig. 2(c)), while the new model is composed of two concentric cylinders with radii of r_1 and r_2 respectively (see Fig. 2(d)). The fiber contents in the two models are

$$V_{f(a)} = \frac{\pi r_1^2 h}{(2l)^2 h} = \frac{\pi r_1^2}{(2l)^2} \tag{1}$$

$$V_{f(b)} = \frac{\pi r_1^2 h}{\pi r_2^2 h} = \frac{r_1^2}{r_2^2} \tag{2}$$

According to the assumption, both models have the same fiber volume fraction V_f, that is

$$V_{f(a)} = V_{f(b)} \Rightarrow 2l = \sqrt{\pi} r_2 \tag{3}$$

When there is a change of r_2 by Δr_2, the strain in the transverse direction of the cubic model (see Fig. 2(a)) is

$$\varepsilon_{t(a)} = \frac{\Delta(2l)}{2l} = \frac{\sqrt{\pi}(r_2 + \Delta r_2) - \sqrt{\pi} r_2}{\sqrt{\pi} r_2} = \frac{\Delta r_2}{r_2} = \varepsilon_{t(b)} \tag{4}$$

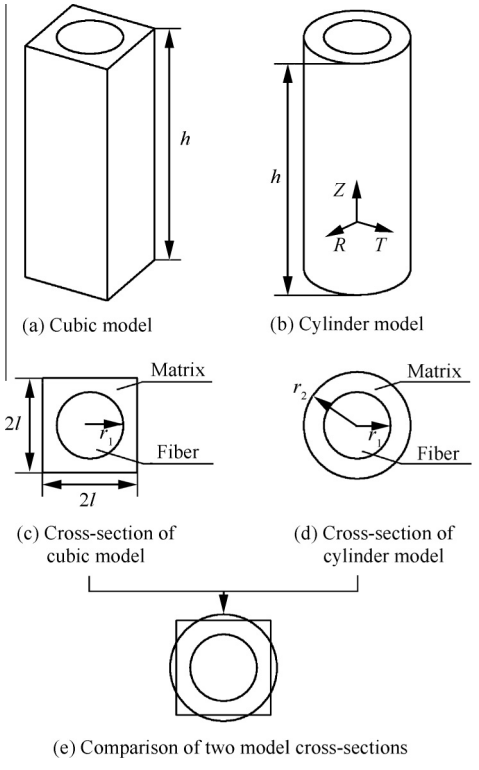

Fig. 2 Transformation of cubic model into cylinder model.

Obviously, both of the two models have the same transverse strain. For axial strains, they are proved to be the same as well in the following section.

2.2. Effective CTE analysis

The theoretical analysis of effective CTEs for a UD composite is based upon the following assumptions:

(1) The cylinder model is composed of two phases (fiber and matrix), ignoring the effect of their interface.
(2) The fiber is regarded as transversely isotropic while the matrix is isotropic.
(3) The cylinder model undergoes a uniform temperature change from T_0 (stress-free temperature) to $T_0 + \Delta T$.
(4) Compared to the height of the RVE h, the length of the UD composite is infinitely long. Therefore, any cross-section of the RVE remains planar when temperature changes, which means that the cylinder model is in an equal strain status in the longitudinal direction.

The transversely isotropic fiber is characterized by the following seven independent thermo-elastic constants: E_{f1} (the axial elastic modulus (Z direction in Fig. 2(b))), E_{f2} (the transverse elastic modulus (RT plane)), G_{f12} (the axial shear modulus), υ_{12} (the axial Poisson's ratio), υ_{23} (the transverse Poisson's ratio), α_{f1} (the axial CTE), and α_{f2} (the transverse CTE).

For the isotropic matrix, it is characterized by the following constants: E_m (the elastic modulus), υ_m (the Poisson's ratio), and α_m (the CTE).

The subscripts "f" and "m" denote fiber and matrix, while 1, 2, 3 refer to axes Z, R, T, respectively. Meanwhile, axial and radial CTEs of the concentric model are designated as α_1 and α_2.

According to the assumption that the transverse section of the concentric cylinder model keeps planar when the temperature changes by ΔT, together with that α_{f1} and α_m are always different in value, thus there exist stresses between the fiber and the matrix in the axial direction, which are denoted by σ_{f1} and σ_{m1}, and the following equations are obtained:

Axial (Z) direction balance equation is

$$\sigma_{f1}\pi r_1^2 + \sigma_{m1}\pi(r_2^2 - r_1^2) = 0 \tag{5}$$

Physics equations are

$$\begin{cases} \varepsilon_1 = \alpha_1 \Delta T \\ \varepsilon_{f1} = \dfrac{\sigma_{f1}}{E_{f1}} + \alpha_{f1}\Delta T \\ \varepsilon_{m1} = \dfrac{\sigma_{m1}}{E_m} + \alpha_m \Delta T \end{cases} \tag{6}$$

To simplify this work, physics equations ignore the Poisson's effect that is caused by the transverse stresses of both the fiber and the matrix.

Geometrics equations is

$$\varepsilon_1 = \varepsilon_{f1} = \varepsilon_{m1} \tag{7}$$

$$\begin{cases} V_f = \dfrac{r_1^2}{r_2^2} \\ V_m = 1 - V_f = \dfrac{r_2^2 - r_1^2}{r_2^2} \end{cases} \tag{8}$$

Eq. (7) is the formulization of Assumption 4 that both the fiber and the matrix have the same strain in the axial direction, while Eq. (8) represents a concise method of calculating the volume fractions of the fiber and the matrix.

Solving Eqs. (5)–(8), the axial CTE of the UD composite is

$$\alpha_1 = \frac{E_{f1}V_f\alpha_{f1} + E_m V_m \alpha_m}{E_{f1}V_f + E_m V_m} \tag{9}$$

Explicit analytical formula Eq. (9) presented here enables the axial CTE of the concentric cylinder model to be predicted in terms of the properties of its constituents and the fiber volume fraction. We can also find that this formula behaves similarly as Schapery's equation.[7]

For the transverse CTE of the cylinder model, it will be analyzed by three-dimensional thermo-elastic mechanics.

According to Assumption (3), the spatial axial symmetry model (see Fig. 2(b)) undergoes a uniform temperature change, and the materials are transversely isotropic. As a result, there is no displacement in the T direction for both the fiber and the matrix, suppose angle θ is an arbitrarily angle in T direction, the radial displacement functions u_f and u_m are independent of angle θ and only related to radius r, and $\tau_{r\theta} = 0$ for both the fiber and the matrix.

From Assumption (4), we can see that the fiber and the matrix share the same axial displacement function ω. Because of spatial axial symmetry and Assumption (4), we have $\tau_{zr} = 0$ and $\tau_{\theta z} = 0$ for both the fiber and the matrix.

The physics equation for this transversely isotropic fiber is

$$\begin{bmatrix} \sigma_{fr} \\ \sigma_{f\theta} \\ \sigma_{fz} \end{bmatrix} = \begin{bmatrix} c_{11} & c_{12} & c_{13} \\ c_{12} & c_{11} & c_{13} \\ c_{13} & c_{13} & c_{11} \end{bmatrix} \begin{bmatrix} \varepsilon_{fr} - \alpha_{f2}\Delta T \\ \varepsilon_{f\theta} - \alpha_{f2}\Delta T \\ \varepsilon_{fz} - \alpha_{f1}\Delta T \end{bmatrix} \tag{10}$$

where c_{ij} ($i, j = 1, 2, 3$) is the fiber degradation stiffness.

The physics equation for the isotropic matrix is

$$\begin{bmatrix} \sigma_{mr} \\ \sigma_{m\theta} \\ \sigma_{mz} \end{bmatrix} = \begin{bmatrix} q_{11} & q_{12} & q_{12} \\ q_{12} & q_{11} & q_{12} \\ q_{12} & q_{12} & q_{11} \end{bmatrix} \begin{bmatrix} \varepsilon_{mr} - \alpha_m\Delta T \\ \varepsilon_{m\theta} - \alpha_m\Delta T \\ \varepsilon_{mz} - \alpha_m\Delta T \end{bmatrix} \tag{11}$$

where q_{ij} ($i, j = 1, 2, 3$) is the matrix degradation stiffness.

Meanwhile, by substituting the properties of the fiber and the matrix, the results are

$$\begin{bmatrix} c_{11} \\ c_{12} \\ c_{13} \\ c_{33} \end{bmatrix} = k \begin{bmatrix} 1 - \upsilon_{12}\upsilon_{21} \\ \upsilon_{12}\upsilon_{21} + \upsilon_{23} \\ \upsilon_{12}(1 + \upsilon_{23}) \\ \upsilon_{12}(1 - \upsilon_{23}^2)/\upsilon_{21} \end{bmatrix} \tag{12}$$

where $k = \dfrac{E_{f2}}{(1 + \upsilon_{23})(1 - \upsilon_{23} - 2\upsilon_{12}\upsilon_{21})}$

$$\begin{bmatrix} q_{11} \\ q_{12} \end{bmatrix} = \frac{E_m}{1 + \upsilon_m} \begin{bmatrix} 1 - \upsilon_m \\ \upsilon_m \end{bmatrix} \tag{13}$$

The geometric equation for this spatial axial symmetry model is

$$\begin{bmatrix} \varepsilon_{ir} \\ \varepsilon_{i\theta} \\ \varepsilon_{iz} \\ \tau_{izr} \end{bmatrix} = \begin{bmatrix} \dfrac{\partial u_i}{\partial r} \\ \dfrac{u_i}{r} \\ \dfrac{\partial \omega_i}{\partial z} \\ \dfrac{\partial \omega_i}{\partial r} + \dfrac{\partial u_i}{\partial z} \end{bmatrix} \quad (i = \mathrm{f}, \mathrm{m}) \tag{14}$$

For this special model, because of low densities of both constituents, the volume force can be ignored, so the equivalent equations are

$$\frac{\partial \sigma_{ir}}{\partial r}+\frac{\partial \tau_{izr}}{\partial z}+\frac{\sigma_{ir}-\sigma_{i\theta}}{r}=0 \quad (i=\mathrm{f},\mathrm{m}) \tag{15}$$

$$\frac{\partial \sigma_{iz}}{\partial r}+\frac{\partial \tau_{izr}}{\partial z}+\frac{\tau_{irz}}{r}=0 \quad (i=\mathrm{f},\mathrm{m}) \tag{16}$$

From Eqs. (10), (14) and (15), we obtain

$$\begin{aligned}&\frac{\partial \sigma_{\mathrm{f}r}}{\partial r}+\frac{\partial \tau_{\mathrm{f}zr}}{\partial z}+\frac{\sigma_{\mathrm{f}r}-\sigma_{\mathrm{f}\theta}}{r}=0\\ &\Rightarrow \frac{\partial \sigma_{\mathrm{f}r}}{\partial r}+\frac{\sigma_{\mathrm{f}r}-\sigma_{\mathrm{f}\theta}}{r}=0\\ &\Rightarrow c_{11}\frac{\partial^2 u_{\mathrm{f}}}{\partial r^2}+\frac{c_{11}}{r}\cdot\frac{\partial u_{\mathrm{f}}}{\partial r}-\frac{c_{11}}{r^2}u_{\mathrm{f}}=0\end{aligned} \tag{17}$$

Since $c_{11}=k(1-\upsilon_{12}\upsilon_{21})\neq 0$ and u_{f} is independent of θ and z, the following result can be obtained:

$$\begin{aligned}&\frac{\mathrm{d}^2 u_{\mathrm{f}}}{\mathrm{d}r^2}+\frac{1}{r}\cdot\frac{\mathrm{d}u_{\mathrm{f}}}{\mathrm{d}r}-\frac{u_{\mathrm{f}}}{r^2}=0\\ &\Rightarrow u_{\mathrm{f}}=A_1 r+\frac{A_2}{r}\end{aligned} \tag{18}$$

Here and the following A_j (j = 1, 2, ..., 8) are constants to be specified.

From Eqs. (10), (14) and (16), we get

$$\begin{aligned}&\frac{\partial \sigma_{\mathrm{f}z}}{\partial r}+\frac{\partial \tau_{\mathrm{f}zr}}{\partial z}+\frac{\tau_{\mathrm{f}rz}}{r}=0\\ &\Rightarrow \omega_{\mathrm{f}}=A_3 z+A_4\end{aligned} \tag{19}$$

Likewise, from Eqs. (11), (14), (15) and (16), we have

$$\begin{aligned}&\frac{\partial \sigma_{\mathrm{m}r}}{\partial r}+\frac{\partial \tau_{\mathrm{m}zr}}{\partial z}+\frac{\sigma_{\mathrm{m}r}-\sigma_{\mathrm{m}\theta}}{r}=0\\ &\Rightarrow u_{\mathrm{m}}=A_5 r+\frac{A_6}{r}\end{aligned} \tag{20}$$

$$\begin{aligned}&\frac{\partial \sigma_{\mathrm{m}z}}{\partial r}+\frac{\partial \tau_{\mathrm{m}zr}}{\partial z}+\frac{\tau_{\mathrm{m}rz}}{r}=0\\ &\Rightarrow \omega_{\mathrm{m}}=A_7 z+A_8\end{aligned} \tag{21}$$

As discussed above, the fiber and the matrix share the same axial displacement function ω, and thus

$$\omega_{\mathrm{m}}=\omega_{\mathrm{f}}=A_3 z+A_4 \tag{22}$$

Boundary conditions:

At $r=0$, for this spatial axial symmetry model, u_{f} must be zero. Thus $A_2=0$ and $u_{\mathrm{f}}=A_1 r$.

At $r=r_1$, here is the interface between the fiber and the matrix. Firstly, their radius displacements must be continuous, that is, $u_{\mathrm{f}(r=r_1)}=u_{\mathrm{m}(r=r_1)}$.

$$\begin{aligned}&A_1 r_1=A_5 r_1+\frac{A_6}{r_1}\\ &\Rightarrow A_6=(A_1-A_5)r_1^2\end{aligned} \tag{23}$$

Secondly, in the interface, the pressure between the fiber and the matrix must be equivalent, that is, $\sigma_{\mathrm{f}r(r=r_1)}=\sigma_{\mathrm{m}r(r=r_1)}$.

By substituting Eqs. (10) and (11), the result is

$$\begin{aligned}&\begin{bmatrix}c_{11}\\c_{12}\\c_{13}\end{bmatrix}^{\mathrm{T}}\begin{bmatrix}A_1-\alpha_{\mathrm{f}2}\Delta T\\A_1-\alpha_{\mathrm{f}2}\Delta T\\A_3-\alpha_{\mathrm{f}1}\Delta T\end{bmatrix}=\begin{bmatrix}q_{11}\\q_{12}\\q_{12}\end{bmatrix}^{\mathrm{T}}\begin{bmatrix}A_5-\frac{A_6}{r_1^2}-\alpha_{\mathrm{m}}\Delta T\\A_5+\frac{A_6}{r_1^2}-\alpha_{\mathrm{m}}\Delta T\\A_3-\alpha_{\mathrm{m}}\Delta T\end{bmatrix}\\ &\Rightarrow (c_{11}+c_{12}+q_{11}-q_{12})A_1+(c_{13}-q_{12})A_3-2q_{11}A_5\\ &\quad=(c_{11}+c_{12})\alpha_{\mathrm{f}2}\Delta T+c_{13}\alpha_{\mathrm{f}1}\Delta T-(q_{11}+2q_{12})\alpha_{\mathrm{m}}\Delta T\end{aligned} \tag{24}$$

At $r=r_2$, the outer cylinder surface of the matrix is a free face, and it suffers nothing, so that $\sigma_{\mathrm{m}r(r=r_2)}=\begin{bmatrix}q_{11}\\q_{12}\\q_{12}\end{bmatrix}^{\mathrm{T}}\begin{bmatrix}A_5-\frac{A_6}{r_2^2}-\alpha_{\mathrm{m}}\Delta T\\A_5+\frac{A_6}{r_2^2}-\alpha_{\mathrm{m}}\Delta T\\A_3-\alpha_{\mathrm{m}}\Delta T\end{bmatrix}$.

By substituting Eqs. (8) and (23), the result is

$$\begin{aligned}&(q_{12}-q_{11})V_{\mathrm{f}}A_1+q_{12}A_3+(q_{11}+q_{11}V_{\mathrm{f}}+q_{12}-q_{12}V_{\mathrm{f}})A_5\\ &\quad=(q_{11}+2q_{12})\alpha_{\mathrm{m}}\Delta T\end{aligned} \tag{25}$$

In the axial direction, the forces that are perpendicular to the cross-section of the concentric model must be equivalent, that is

$$\sum F_{\mathrm{f}z}+\sum F_{\mathrm{m}z}=0 \tag{26}$$

$$\begin{aligned}\sum F_{\mathrm{f}z}&=\int_0^{r_1}\int_0^{2\pi}\sigma_{\mathrm{f}z}r\,\mathrm{d}r\mathrm{d}\theta\\ &=\int_0^{r_1}r\int_0^{2\pi}\begin{bmatrix}c_{13}\\c_{13}\\c_{33}\end{bmatrix}^{\mathrm{T}}\begin{bmatrix}A_1-\alpha_{\mathrm{f}2}\Delta T\\A_1-\alpha_{\mathrm{f}2}\Delta T\\A_3-\alpha_{\mathrm{f}1}\Delta T\end{bmatrix}\mathrm{d}r\mathrm{d}\theta\end{aligned} \tag{27}$$

$$\begin{aligned}\sum F_{\mathrm{m}z}&=\int_{r_1}^{r_2}\int_0^{2\pi}\sigma_{\mathrm{m}z}r\,\mathrm{d}r\mathrm{d}\theta\\ &=\int_{r_1}^{r_2}r\int_0^{2\pi}\begin{bmatrix}q_{12}\\q_{12}\\q_{11}\end{bmatrix}^{\mathrm{T}}\begin{bmatrix}A_5-\frac{A_6}{r^2}-\alpha_{\mathrm{m}}\Delta T\\A_5+\frac{A_6}{r^2}-\alpha_{\mathrm{m}}\Delta T\\A_3-\alpha_{\mathrm{m}}\Delta T\end{bmatrix}\mathrm{d}r\mathrm{d}\theta\end{aligned} \tag{28}$$

Thus

$$\begin{aligned}&\sum F_{\mathrm{f}z}+\sum F_{\mathrm{m}z}=0\\ &\Rightarrow 2c_{13}V_{\mathrm{f}}A_1+[c_{33}V_{\mathrm{f}}+(1-V_{\mathrm{f}})q_{11}]A_3+2q_{12}(1-V_{\mathrm{f}})A_5\\ &=2c_{13}V_{\mathrm{f}}\alpha_{\mathrm{f}2}\Delta T+c_{33}V_{\mathrm{f}}\alpha_{\mathrm{f}1}\Delta T+(1-V_{\mathrm{f}})(2q_{12}+q_{11})\alpha_{\mathrm{m}}\Delta T\end{aligned} \tag{29}$$

Eqs. (24), (25) and (29) can be combined into the following form:

$$\boldsymbol{BA}=\boldsymbol{D} \tag{30}$$

Therein,

$$\boldsymbol{B}=[\boldsymbol{B}_1\quad \boldsymbol{B}_2\quad \boldsymbol{B}_3]$$

$$\boldsymbol{A}=[A_1\quad A_3\quad A_5]^{\mathrm{T}}$$

$$\boldsymbol{B}_1=\begin{bmatrix}c_{11}+c_{12}+q_{11}-q_{12}\\(q_{12}-q_{11})V_{\mathrm{f}}\\2c_{13}V_{\mathrm{f}}\end{bmatrix}$$

$$\mathbf{B}_2 = \begin{bmatrix} c_{13} - q_{12} \\ q_{12} \\ c_{33}V_f + q_{11}(1 - V_f) \end{bmatrix}$$

$$\boldsymbol{B}_3 = \begin{bmatrix} -2q_{11} \\ q_{11}(1 + V_f) + q_{12}(1 - V_f) \\ 2q_{12}(1 - V_f) \end{bmatrix}$$

$$\boldsymbol{D} = \Delta T \begin{bmatrix} (c_{11} + c_{12})\alpha_{f2} + c_{13}\alpha_{f1} - (q_{11} + 2q_{12})\alpha_m \\ (q_{11} + 2q_{12})\alpha_m \\ 2c_{13}V_f\alpha_{f2} + c_{33}V_f\alpha_{f1} + (2q_{12} + q_{11})(1 - V_f)\alpha_m \end{bmatrix}$$

So, $\boldsymbol{A} = \boldsymbol{B}^{-1}\boldsymbol{D}$.

At $r = r_2$, the radius displacement of this concentric model is

$$\begin{aligned} u_{m(r=r_2)} &= A_5 r_2 + \frac{A_6}{r_2} = A_5 r_2 + \frac{(A_1 - A_5)r_1^2}{r_2} \\ &= r_2[A_5 + (A_1 - A_5)V_f] = r_2[A_1 V_f + A_5 V_m] \end{aligned} \tag{31}$$

The CTE is defined as $\alpha = \dfrac{\Delta l}{l\,\Delta T}$ for a dimension of l, so the transverse CTE of this RVE is

$$\begin{aligned} \alpha_2 &= \frac{\Delta r_2}{r_2 \Delta T} = \frac{u_{m(r=r_2)}}{r_2 \Delta T} = \frac{A_1 V_f + A_5 V_m}{\Delta T} \\ &= a_m + \frac{d_1 + d_2}{n_1 + n_2 + n_3} \end{aligned} \tag{32}$$

Therein,

$$\begin{cases} d_1 = E_{f1}E_{f2}V_f\upsilon_{12}\left[(\upsilon_m^2 + \upsilon_m V_m)(\alpha_m - \alpha_{f1}) \right. \\ \qquad \left. +2V_f(\alpha_{f2} - \alpha_m) + \upsilon_m^2 V_f(\alpha_m + \alpha_{f1} - 2\alpha_{f2})\right] \\ d_2 = E_{f1}E_m V_f[2\upsilon_{21}V_m(1 - \upsilon_m\upsilon_{12})(\alpha_m - \alpha_{f2}) \\ \qquad +\upsilon_{12}V_m(2\upsilon_{21} - \upsilon_m + \upsilon_m^2)(\alpha_m - \alpha_{f1})] \\ n_1 = E_m E_{f1} V_m[\upsilon_{21} + (\upsilon_{21} + \upsilon_{12})V_f \\ \qquad +\upsilon_m\upsilon_{21}V_m - (1 + 4\upsilon_{21})\upsilon_m\upsilon_{12}V_f] \\ n_2 = E_m^2 V_m^2 \upsilon_{12}(1 - \upsilon_m - 2\upsilon_{12}\upsilon_{21}) \\ n_3 = E_{f1}E_{f2}V_f\upsilon_{12}(1 + V_f - 2\upsilon_m^2 V_f + \upsilon_m V_m) \end{cases}$$

According to Eq. (4) and the definition of CTE, both the cubic model and the concentric model have the same strain and CTE in the transverse direction. Eq. (9) shows that the axial CTE is independent of the shape of the cross-section of this RVE. Therefore, the axial and transverse CTEs for Fig. 2(a) are α_1 and α_2 which are shown in Eqs. (9) and (32) that are derived by the model in Fig. 2(b) .

3. Material and FE model

Here the FEM is adopted to determine both axial and transverse CTEs of the UD fiber-reinforced composite through the cubic model (see Fig. 2(a)) and the concentric model (see Fig. 2(b)). For the advantages of symmetry, only a quarter of each RVE is modeled. As shown, Fig. 3(a) and (b) correspond to the cubic and concentric models, respectively. CTE predictions by the analytical method and the FEM are compared with experimental data to justify the simplification of cubic to cylinder model and analytical results.

The FE models are created by MSC. Patran 2010 with an 8-node hexahedral element, and then submitted to MD. Nastran for computation. Each model is created according to different fiber–matrix combinations and fiber volume fractions. The dimension of each FE model in Z direction has a unit length, while X and Y dimensions may change with different material systems. However, for a given fiber–matrix combination, Fig. 3(a) and (b) share the same fiber radius and fiber volume fraction.

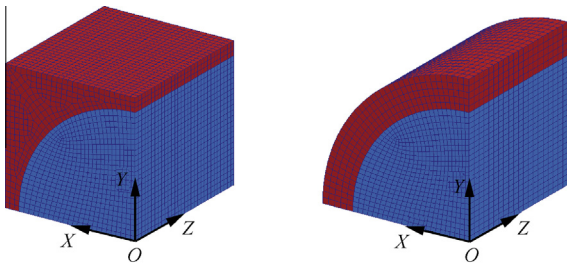

(a) Cubic FE model (b) Cylinder FE model

Fig. 3 FE models.

Boundary conditions for the FE models are as follows: (1) nodes that in the plane XOY and $Z = 0$ are restricted to move in X and Y directions; (2) node at $X = Y = Z = 0$ is fixed, and allows no displacement; (3) the planes that are parallel to X, Y, and $Z = 0$ keep planar and remain parallel to their original positions when in deformation; (4) the initial temperature is assumed to be room temperature and ΔT is 1 °C.

Material properties for the FE models are shown in Tables 1 and 2. The data are extracted from the study by Bowles and Tompkins.[16] In their investigation, all matrices are isotropic while fibers are transversely isotropic. Meanwhile, all data are used in analytical solutions Eqs. (9) and (32).

4. Results and discussion

From the properties of constituents listed in Tables 1 and 2, it can be found that the UD fiber-reinforced composite material systems have an axial fiber to matrix stiffness ratio (E_{f1}/E_m) ranging from 6 to 140, and an axial fiber to matrix CTE ratio (α_{f1}/α_m) ranging from −0.01 to −0.30. As a result, the present study covers a wide range of fiber/matrix combinations.

Comparisons among predicted CTEs of the concentric cylinder model, experiments, and some other analytical solutions, including modified Schapery's equation,[2] Chamberlain's equation,[1] Chamis and Scheider's equation,[1] are carried out. Fig. 4 shows a comparison of predicted longitudinal CTEs of eight fiber–matrix combinations, which are predicted by the concentric cylinder model. Experimental data, the FEM, and some analytical methods predicted results are shown in Table 3. The concentric cylinder model (CM), Schapery (SH), Chamberlain (CB), and Chamis & Scheider (CH) solutions all share the same Eq. (9) to predict longitudinal CTEs, and their predicted data are listed in the same column in Table 3. In the last two columns, FEM-cubic and FEM-cylinder stand for two different FE models which are shown in Fig. 3. The difference between FEM-cubic and FEM-cylinder results of each material combination is almost negligible except T300/5208, given the accuracy of numerical computation, which means that the FE models in Fig. 3(a) and (b) are equivalent in predicting the axial CTE.

The mean square error of cylinder model predictions relative to experimental results is 8.55×10^{-8}/°C, which is much smaller compared to the predicted CTEs. That means all the predictions

Table 1 Properties of fibers at room temperature.[16]

Fiber	E_1 (GPa)	E_2 (GPa)	G_{12} (GPa)	G_{23} (GPa)	v_{12}	v_{23}	α (10^{-6}/°C)	
							α_1	α_2
T300	233.04	23.10	8.96	8.27	0.20	0.40	−0.54	10.08
C6000	233.04	23.10	8.96	8.27	0.20	0.40	−0.54	10.08
HMS	379.21	6.21	7.58	2.21	0.20	0.40	−0.99	6.84
P75	550.20	9.51	6.89	3.38	0.20	0.40	−1.35	6.84
P100	796.34	7.24	6.89	2.62	0.20	0.40	−1.404	6.84

Table 2 Properties of matrices at room temperature.[16]

Matrix	E (GPa)	G (GPa)	v	α (10^{-6}/°C)
934 epoxy	4.34	1.59	0.37	43.92
5208 epoxy	4.34	1.59	0.37	43.92
930 epoxy	4.34	1.59	0.37	43.92
CE339 epoxy	4.34	1.59	0.37	63.36
PMR15 polyimide	3.45	1.31	0.35	36.00
2024 aluminum	73.08	27.58	0.33	23.22
Borosilicate glass	62.74	26.20	0.20	3.24

are in good agreement with experimental results. Although errors exist, the general response behaves similarly (decreasing longitudinal CTEs with increasing fiber volume fraction). It indicates that the relative magnitudes of fiber/matrix stiffness ratio and CTE ratio do not significantly affect the general trend in longitudinal CTEs. Furthermore, we can find that for the same material system, such as T300/5208, T300/934, and C6000-Pi, the larger CTE of the matrix, the more dramatically the CTE of composite decrease until V_f exceeds 0.6. For the same matrix, the larger modulus and absolute value of the axial CTE of the fiber, the more dramatic decrease in the longitudinal CTE of such a material combination (e.g., T300/934, P75/934).

It can be seen from Eq. (9) that the longitudinal CTE is determined by both the fiber and the matrix. Usually, the CTE of the matrix is much larger than that of the fiber, so the upper and lower bounds of α_1 are the CTE of the matrix and the longitudinal CTE of the fiber, respectively. When the fiber content is low, e.g., $V_f \leqslant 0.15$, α_1 is dominated by the CTE of the matrix, because the volume fraction and CTE of the matrix are much larger than those of the fiber; while the fiber content is somewhat higher, e.g., $V_f \geqslant 0.5$, α_1 is mostly determined by the thermal property of the fiber, because the stiffness of the fiber in the longitudinal direction is quite larger than that of the matrix. Such a phenomenon could be found in Fig. 4 directly as well.

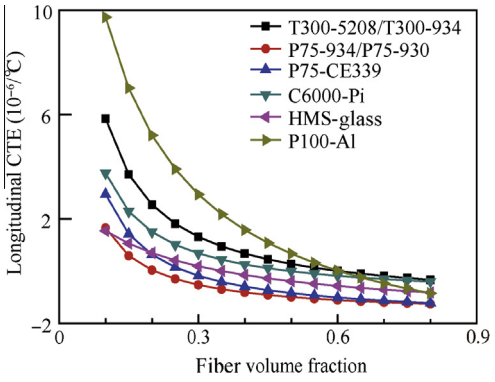

Fig. 4 Predicted longitudinal CTE vs fiber volume fraction.

Fig. 5 shows the response of transverse CTEs as a function of fiber volume fraction for different fiber–matrix combinations. Experimental data and FEM results are also shown in the figures mentioned above as well as in Table 4. In Table 4, it can be found that the FEM-cubic and FEM-cylinder results for different material combinations are almost the same, the maximum error between the FEM-cubic and FEM-cylinder predictions is 0.489×10^{-6}/°C for C6000-Pi material, and the maximum relative error is less than 2.5%. Such good agreements mean that the equivalent process of Fig. 2(a) to (b) in the transverse direction is reasonable.

Errors between the FEM results and the concentric cylinder model predictions still exist. A possible reason lies in the assumptions and simplifications of the concentric cylinder model. However, the predictions by the concentric model are in much better agreement with experimental data than those by other solutions. The maximum error between the concentric cylinder model and experimental results is 5.672×10^{-6}/°C, while the maximum error between the FEM-cubic and experimental results is 6.748×10^{-6}/°C. The minimal errors of the concentric cylinder model and FEM predictions are 0.079×10^{-6}/

Table 3 Comparison of experimental and analytical data for the longitudinal CTE.

Material systems	Longitudinal CTE (10^{-6}/°C)			
	Experiment	CH, CM, SH, CB	FEM-cubic	FEM-cylinder
T300/5208	−0.113	−0.153	−0.068	−0.092
T300/934	−0.002	0.076	0.171	0.166
P75/934	−1.051	−0.965	−0.920	−0.922
P75/930	−1.076	−1.157	−1.125	−1.129
P75/CE339	−1.021	−0.916	−0.857	−0.859
C6000/Pi	−0.212	−0.225	−0.175	−0.187
HMS/Glass	−0.414	−0.324	−0.324	0.324
P100/Al	1.440	1.575	1.634	1.634

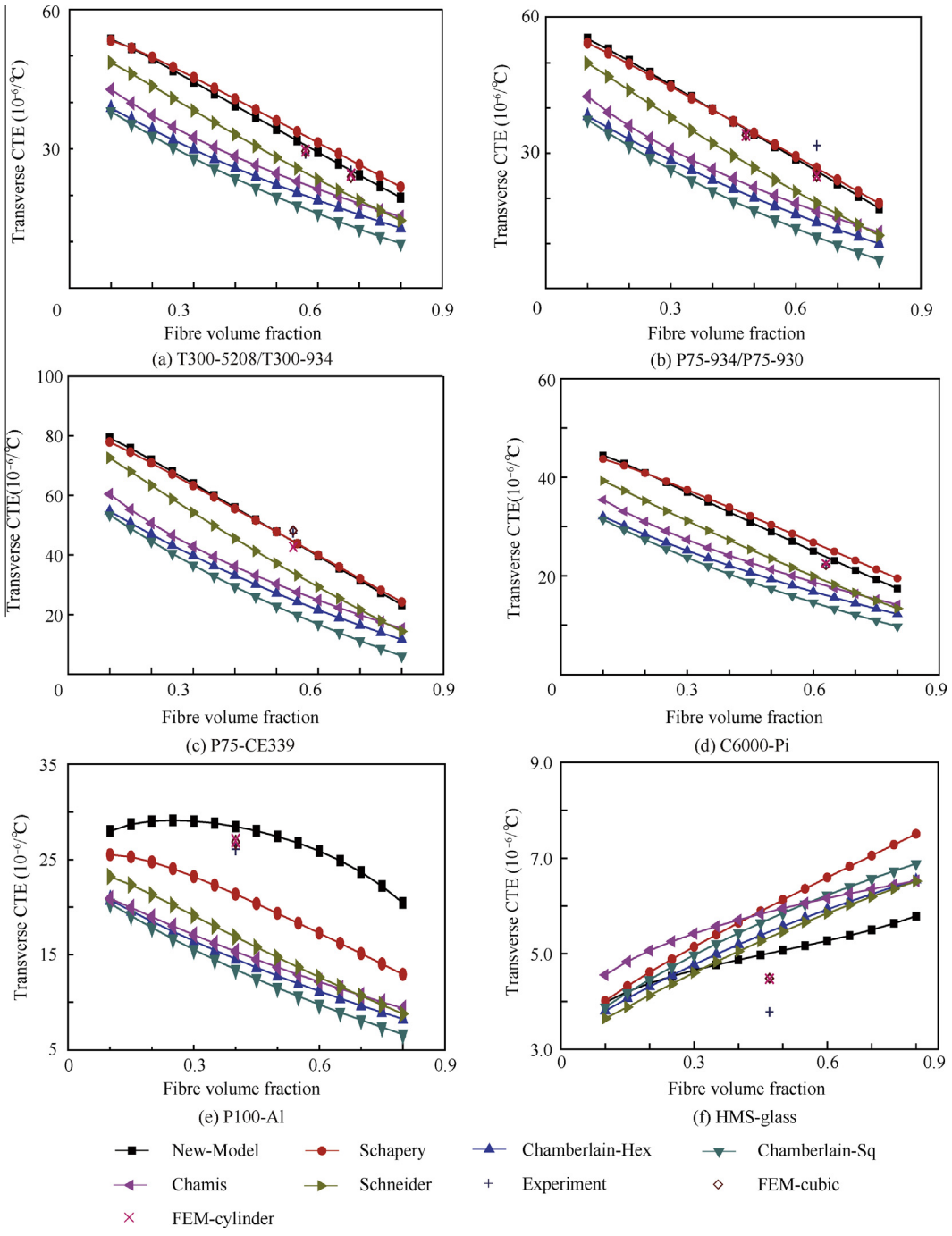

Fig. 5 Transverse CTE of different composite materials.

Table 4 Comparison of experimental and analytical data of transverse CTE.

Material systems	Transverse CTE (10^{-6}/°C)							
	Experiment	CM	SH	CH	CB-Hex	CB-Sq	FEM-cubic	FEM-cylinder
T300/5208	25.236	25.315	27.518	18.841	16.432	13.360	23.967	24.433
T300/934	29.034	30.749	32.747	22.298	19.908	17.098	29.457	29.583
P75/934	34.524	35.350	35.507	23.180	20.918	18.131	34.042	34.047
P75/930	31.716	26.044	26.696	17.161	14.769	11.489	24.968	25.025
P75/CE339	47.412	44.518	44.617	28.190	24.847	20.304	42.709	42.703
C6000/Pi	22.428	23.854	25.661	18.004	16.051	13.808	22.039	22.529
HMS/Glass	3.780	5.011	5.983	5.881	5.463	5.728	4.486	4.477
P100/Al	26.118	28.492	21.375	15.336	14.549	13.448	26.865	27.002

°C and 0.101×10^{-6}/°C. There are eight material combinations in total in this research, and the compared results in Table 4 show that six out of eight predictions by the concentric cylinder model are in better agreement with experimental data than those by other solutions; for the other two material combinations (P75/934 and P75/930), the results predicted by concentric cylinder model and Schapery model are almost the same, and the predictions are quite close to the experimental data as well.

As seen in Fig. 5, unlike the axial CTE, the response of the transverse CTE as a function of fiber volume fraction is affected by both the fiber to matrix stiffness ratio (E_{f2}/E_m) and the transverse CTE ratio (α_{f2}/α_m). P100-Al has a similar transverse CTE ratio ($\alpha_{f2}/\alpha_m < 1$) with T300-5208/934, P75-934/930, P75-CE339, and C6000-Pi, so the response of α_2 decreases with increasing fiber volume fraction. Meanwhile, P100-Al has a fiber to matrix stiffness ratio ($E_{f2}/E_m < 1$) which is contrary to the other fiber–matrix combinations, and thus the difference between the cylinder model and other solutions in Fig. 5(e) is more apparent than those in Fig. 5(a)–(d). The same phenomenon can be found in Fig. 5(f). For material HMS-glass, the transverse CTE of the fiber is larger than that of the matrix ($\alpha_{f2}/\alpha_m > 1$), which is contrary to the other material combinations. As a result, the response of α_2 increases with increasing fiber volume fraction.

Generally, the transverse CTE of a UD fiber-reinforced composite is determined by both the matrix and the fiber, with the CTE of the matrix as a base, as can be seen in Eq. (32). The transverse CTE is almost linear as the fiber content increases, for which maybe the reason lies in that $E_{f2}\alpha_{f2} \approx E_m\alpha_m$, and the product of the CTE and stiffness of the fiber in the transverse direction is of the same magnitude order as that of the matrix, which means the contributions to the transverse CTE of the UD composite by the fiber and the matrix are at the same level. Therefore, the transverse CTE exhibits quite linearity.

5. Conclusions

(1) The equivalent process of transforming the model in Fig. 2(a) to the one in Fig. 2(b) is reasonable.
(2) Explicit formula Eqs. (9) and (32) for CTE predictions are easy to use and results are in good agreement with experimental data.
(3) The longitudinal CTE of a UD fiber-reinforced composite can be more accurately predicted than the transverse CTE.
(4) As would be expected, both longitudinal and transverse CTEs are mostly affected by the fiber to matrix stiffness ratio (E_{f2}/E_m) and the fiber to matrix CTE ratio (a_{f2}/a_m).

Acknowledgement

Thank Miss YI Xiyuan for her kind help in revising this paper.

References

1. Karadeniz ZH, Kumlutas D. A numerical study on the coefficients of thermal expansion of fiber reinforced composite materials. *J Compos Struct* 2007;**78**(1):1–10.
2. Schapery RA. Thermal expansion coefficients of composite materials based on energy principles. *J Compos Mater* 1968;**2**(3):380–404.
3. Van Fo Fy GA. Thermal strains and stresses in glass fiber-reinforced media. *Prikl Mekh Teor Fiz* 1965;**8**:17 [Russian].
4. Van Fo Fy GA. Elastic constants and thermal expansion of certain bodies with inhomogeneous regular structure. *Soviet Phys Doklady* 1966;**11**:176 [Russian].
5. Van Fo Fy GA. Basic relations of the theory of oriented glass reinforced plastics with hollow fibers. *Mekhanika Polimerov* 1966;**2**:763 [Russian].
6. Levin VM. Thermal expansion coefficients of heterogeneous materials. *Mech Solids* 1967;**2**(1):88–94.
7. Schapery RA. On application of a thermodynamic constitutive equation to various nonlinear materials [dissertation]. West Lafayette: Purdue University; 1968.
8. Rogers KF, Phillips LN, Kingston-Lee DM, Yates B, Overy MJ, Sargent JP, et al. The thermal expansion of carbon fibre-reinforced plastics. Part 1: The influence of fiber type and orientation. *J Mater Sci* 1977;**12**(4):718–34.
9. Chamis CC. Simplified composite micromechanics equations for hygrothermal and mechanical properties. *SAMPE Quart* 1984;**15**(3):14–23.
10. Rosen BW, Hashin Z. Effective thermal expansion coefficients and specific heats of composite materials. *Int J Eng Sci* 1970;**8**(2):157–73.
11. Hashin Z. Analysis of properties of fiber composites with anisotropic constituents. *J Appl Mech* 1979;**46**(3):543–50.
12. Sideridis E. Thermal expansion coefficient of fiber composites defined by the concept of the interphase. *Compos Sci Tech* 1994;**51**(3):301–17.
13. Islam MDR, Sjolind SG, Pramila A. Finite element analysis of linear thermal expansion coefficients of unidirectional cracked composites. *J Compos Mater* 2001;**35**(19), 1762-76.
14. Rupnowski P, Gentza M, Sutterb JK, Kumosa M. An evaluation on the elastic properties and thermal expansion coefficients of medium and high modulus graphite fibers. *Compos A* 2005;**36**(3):327–38.
15. Miled H, Silva L, Agassant JF, Coupea T. Numerical simulation of fiber orientation and resulting thermo-elastic behavior in reinforced thermo-plastics. *Mech Response Compos* 2008;**10**(978):293–313.
16. Bowles DE, Tompkins SS. Prediction of coefficient of thermal expansion for unidirectional composite. *J Compos Mater* 1989;**23**(4):370–88.

Ran Zhiguo is a Ph.D. student in School of Aeronautic Science and Engineering at Beihang University, and is majoring in flying vehicle design. His main research areas include flying vehicle structure design, composite structure design and optimization.

Yan Ying is a professor and Ph.D. advisor in School of Aeronautic Science and Engineering at Beihang University. She received her Ph.D. degree from University of Southampton in 1994. Her current research interests are flying vehicle composite structure design & optimization, aircraft vibration modeling, helicopter crashless, and composite structure repair technology.